DESIGN REPORT

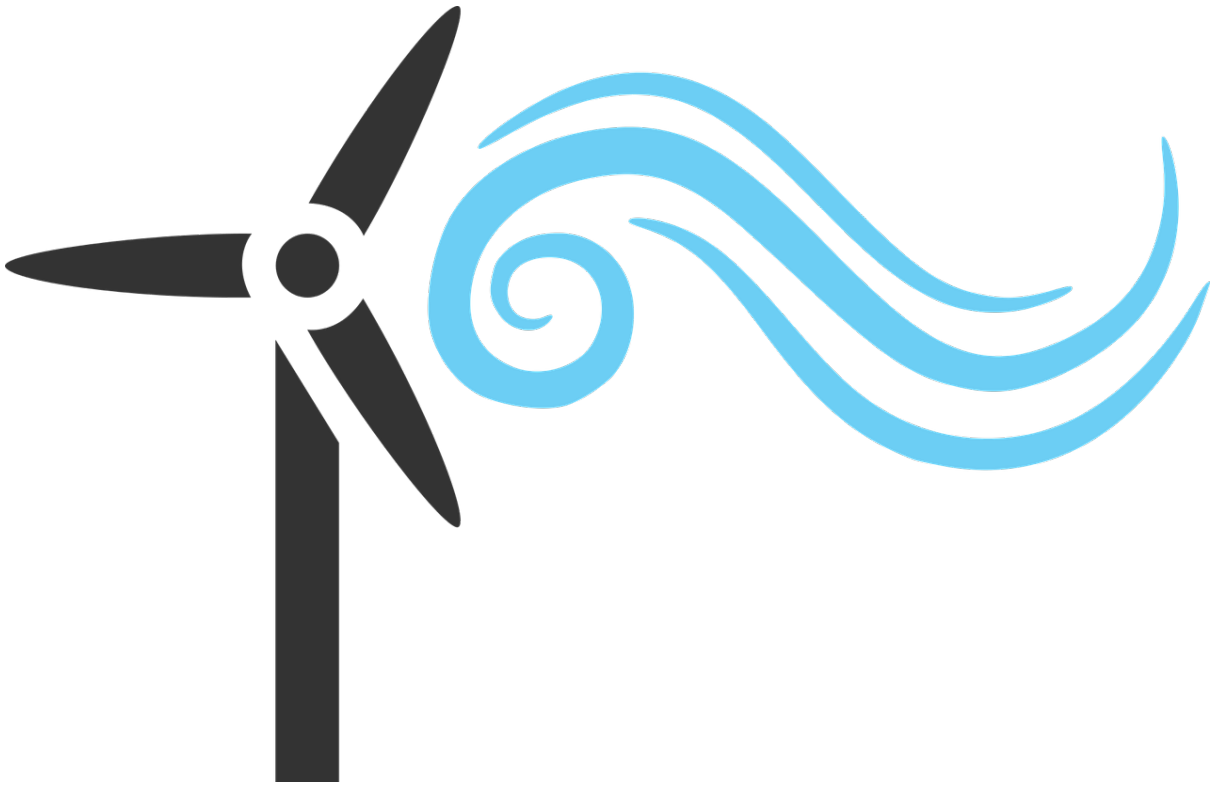

ISWTC 2019

TEAM – DUWT

TU Delft

DUWIND
DELFT UNIVERSITY WIND ENERGY RESEARCH INSTITUTE

Acknowledgements

It gives us great pleasure to present this report, which is a result of several months of work into designing a small wind turbine for ISWTC 2019. The work involved research, design, analysis and also consulting few people who are working in this field. This report would not have been complete without their valuable inputs and guidance.

Firstly, Team DUWT, Delft University Wind Turbine, expresses its heartfelt gratitude to Ir. Daan van der Hoek for his continuous support throughout the team's foundation.

Secondly, the team is grateful to DUWIND (The Delft University Wind Energy Institute) for the financial support and assistance without which the project would not have been possible.

Lastly, the team expresses its gratitude to the organizers of ISWTC 2019 for providing this opportunity and an international platform for the team to be a part of and to showcase new ideas.

Place: Delft, Netherlands
Date: 31 May, 2019

Contents

1 Introduction

"The pessimist complains about the wind; the optimist expects it to change; the realist adjusts the sails." - William Arthur Ward

Innovation is the engine that may power the inevitable energy transition to sustainable energy system and ensure we meet the targets to keep the global average temperature well below 2C. The rising electricity demand, electricity price, support by government for self-production of electricity (so called prosumers) and various advantages over large wind turbines necessitates innovation in the small wind turbines among other small scale renewable sources.

Acknowledging the urgency for innovations in the small wind turbine section in the broad energy technology spectrum and with an ambition to contribute for the same, a group of students from TU Delft have come together to adjust the sails with an aspiration to bring in innovation driven by functionality, robustness and affordability utilizing the platform of ISWTC 2019.

The objective of this report is to study and design a small wind turbine for the International Small Wind Turbine Competition 2019. A team was composed for this task from multiple disciplines and at different stages of their study. Later on, sub teams were formed and tasks were divided and distributed to the team members depending on their affinity, knowledge and skill expertise. The tasks mainly involved design of elements, material selection, design calculations, software simulation tests and design documentation.

A brainstorming session and subsequent research was done to decide on the type of small wind turbine to be designed.

The structure of the report is as follows: the rationale behind the design choice is elaborated in Chapter 2. Chapter 3 provides a detailed assessment of the performance of the turbine basing on computational fluid dynamics. Chapter 4 analyses the specified load cases which is followed by the structural analysis of the turbine components. In the next chapter, the turbine specifications have been documented in detail. Chapter 5 consists of calculations for energy payback time. Chapter 6 concludes the report with key insights.

2

System design

In this chapter, all the design choices are discussed and detailed component description is provided. First section describes the rationale behind the choice of the turbine designed. Second section explains the design approach for the turbine in brief. The chapter is concluded with a third section that describes all the components of the turbine starting from rotor to controller in detail.

2.1. Turbine Choice: Savonius (Vertical Axis Drag Based Turbine)

The Savonius (Vertical Axis Drag Based Wind Turbine) is chosen as DUWT's representative entry for this competition with the motivational reasons discussed in this section. The primary reason for the choice is because there is the opportunity and challenge to derive a creative approach to design in comparison to standard lift based wind turbines. In addition, relatively fewer literature and experimental studies have been made on Savonius wind turbines. This means that the scope of this project has the potential to extend towards contributing, and innovating in performance improvement.

Aside from the motivational reasonings for choosing the Savonius wind turbine, further rationale relevant for the competition are taken into account. Henceforth, this section further discusses the reasonings pertaining to performance and economic feasibility that depicts these factors for the Savonius turbine in comparison to the other types. This process facilitates making a technical decision for choosing the turbine type, taking into account the objectives and constraints provided by the contest organizers.

The comparison models were:

- Lift-based Vertical Axis Wind Turbine (VAWT)
- Horizontal Axis Wind Turbine (HAWT)
- Drag-based Vertical Axis Wind Turbine (Savonius)

The three options considered to highlight the advantages and disadvantages relative to the Savonius wind turbine are listed in Table 2.1.

Type	Advantages	Disadvantages
(Lift-based) VAWT	- Suitable in an urban setting - Many control variations can be implemented in future designs	- High cut-in wind speeds - Relatively higher manufacturing cost
(Lift-based) HAWT	- Higher power coefficient - Well defined control strategy for a range of wind speeds - Multiple design tools readily available	- Relatively higher manufacturing cost - Less suitable in urban setting - Average cut-in speeds - Less scope for innovation
Savonius	- Low cut-in speed - Suitable in an urban setting - Low start-up torques - Relatively lower manufacturing cost - Presents the opportunity to innovate with design approach	- Low power coefficient - Lack of theoretical framework, and reference model for scaling - Low efficiencies compared to HAWTs

Table 2.1: Comparing the Pros & Cons of the three types of turbine

Considering the advantages and disadvantages of the three turbines, it can be observed that the Savonius has a relatively lower power coefficient, and lower efficiency compared to other models. However, it has the advantage of lower manufacturing costs, lower cut-in speed, and lower start-up torques. There also exists the potential for the turbine to have a smaller energy payback period.

A notable drawback and challenge of the Savonius wind turbine is the absence of a reference model. Therefore, the design of the Savonius is dependent on iterative experimental data derived from literature. The numerical results of the teams experiments are also used as supplementary data for the turbine.

2.2. Design Approach

This section elaborates on the applied design approach for the Savonius wind turbine. Due to the unavailability of a structured theoretical framework for design or a reference model tool for scaling, the basic design and dimension choices are made from extensive literature review. The inference of testing and experimental validation data from reference material describing design choices of the turbine's components, provided a guidance for choices to be made for formulating a model satisfying the competition constraints.

The rotor, drive-train, and controller design approaches can be summarized as follows. A rotor configuration is decided based on parameterization of design choices that can influence performance. These parameters are discussed in Section 2.3.1. The performance assessment of variation of these parameters is then carried out through 2D Computational flow analysis, detailed in Chapter 3. Computational Fluid Dynamics (CFD) is used as a design iteration tool for producing the most optimal model. Next comes the design approach for the drive train generator and the gear system. Firstly, the generator selection is based on desired output voltage and rated generator speed. Then, the gear system configuration is made with the objective of amplifying the rotation speed of the rotor to match the rated RPM of the generator at rated wind speed. The details are elaborated in Section 2.3.2.

2.3. Turbine Components

This section aims to give a detailed overview of the design parameters of each component. Graphical visualization of the whole turbine is shown in Figure 2.1 and Figure 2.2. Figure 2.1 shows the rotor assembly and Figure 2.2 shows the lower assembly consisting of the support plates, drive train, braking and bearing assemblies. Each component assembly is described in detail in the following sections.

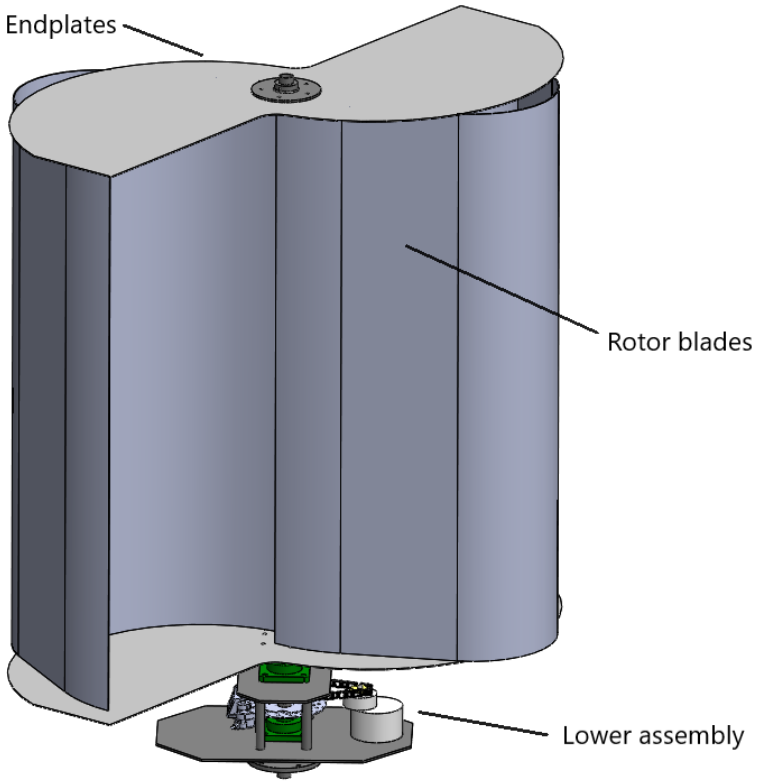

Figure 2.1: Turbine assembly

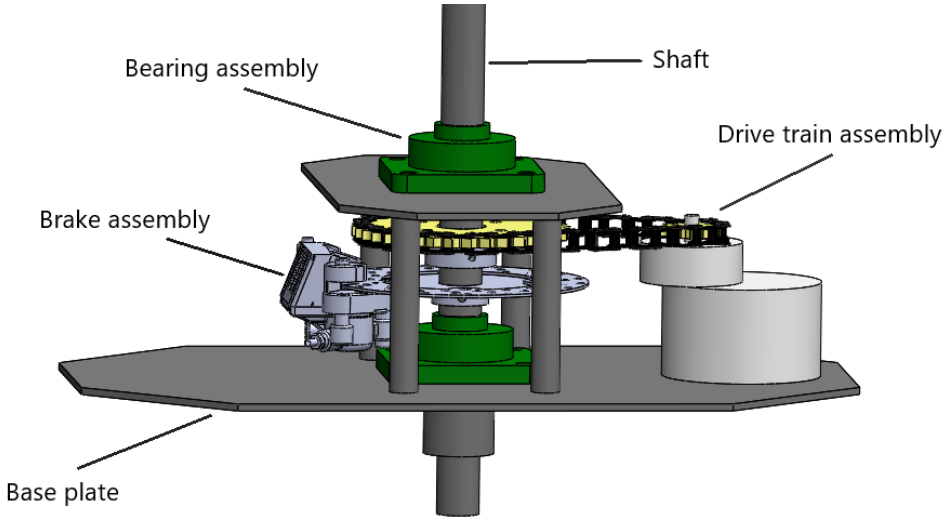

Figure 2.2: Lower assembly

2.3.1. Rotor Design

The rotor design approach, as explained above is an iterative procedure involving utilization of literature guided optimal performance design choices, and implementation after computing flow analysis cases. This section presents the geometric details of the rotor, and the important elements for a Savonius turbine. Table 2.2 summarizes the rotor specifications and Figure 2.3 shows an exploded view of the rotor assembly.

Component	Specification	Value
Rotor	Cup Diameter	68 cm
	Rotor Diameter	130 cm
	Blade height	125 cm
	Aspect ratio	0.96
	Separation distance	6.8 cm
	Gap	0 cm
	Foam width	18 cm
End plate	Area	69 cm^2

Table 2.2: Rotor Specifications

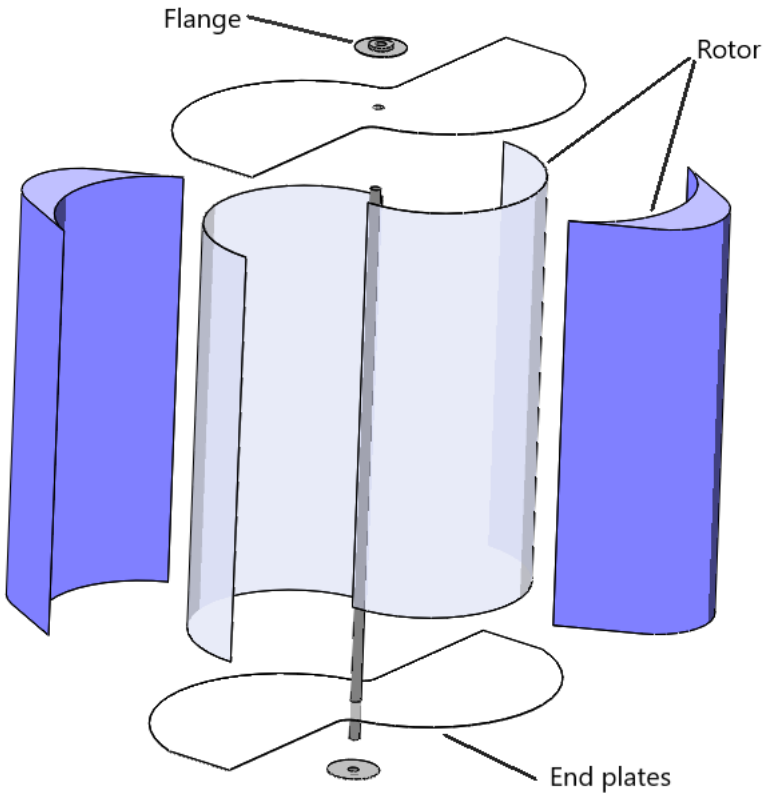

Figure 2.3: Exploded view of the rotor assembly

A top view of a conventional 2 bladed Savonius turbine is shown in Figure 2.4. The rotor design is parametrized into different variables as listed below :

1. **Separation distance** (s): The distance between the inner end of the two cups, or the overlap between the cups. The separation distance will be characterized by the separation ratio (s/d), where d is the diameter of one cup.
2. **Gap** (τ): In the planar view, the vertical distance between the two cups.

3. **Modification of the concave surface** of the turbine: reduces the negative torque. This modification has been made on the rotor through the addition of a contoured surface made of foam. In the remainder of this report, this modification will be refereed to as foam.

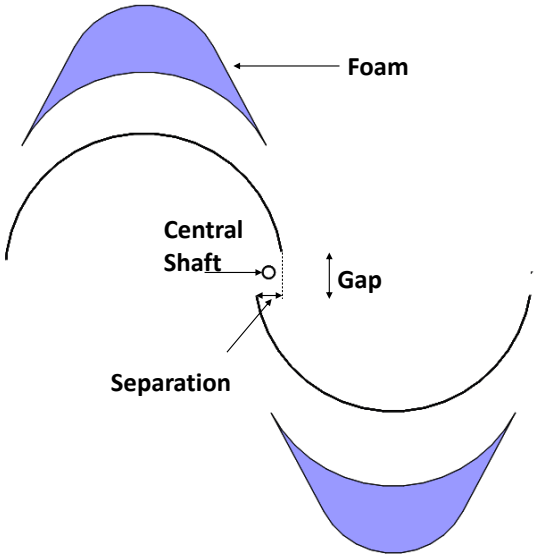

Figure 2.4: Parametrization of the rotor

A lot of theoretical and experimental research is done in the field of Savonius turbines by parameterizing the design into factors like separation distance, aspect ratio, gap, blade arc angle, etc. A comprehensive study about the effect of the blade arc angle on the power coefficient (C_p) conducted by Mao et al [1]. The effect of aspect ratio, number of stages, gap and overlap, on C_p, was consulted using the study by Modi et al [2]. This helped to derive near optimal configuration for an aspect ratio of 0.77, zero gap and an overlap ratio lower than 0.22 is derived. A positive effect of having end plates to cover the blades was reported by Jeon et al [3], wherein the different shapes of the end plates were tried out and compared with a rotor without any capping. Also, various papers on optimization of the conventional blade shape exist. However, the effect of having an external surface on the convex side of the blade, to reduce the negative torque has not been tried out in literature.

For this project, the separation and gap parameters that are to be tried are based on the experimental study conducted by SANDIA labs [4], due to the similarity in dimensions. The height of the rotor is governed by the overall height restrictions based on the competition guidelines. The rotor diameter is decided so as to maximize the aspect ratio and yet, not lose out on the rotor area. The configurations that will be analyzed using Computational fluid dynamics (CFD) simulations are listed in Chapter 3.

2.3.2. Drive Train

The drive train consists of two main components, the generator and the configuration of a gear system to maintain generator's revolution per minute (RPM), at power producing levels. The generator is chosen based on the desired output voltage and the rated speed considering the rotational speed of our turbine. The summary of components is given in Table 2.3 and the drive train is visualized through Figure 2.5.

Component	Specification	Value
Shaft	Diameter	30 mm
Generator (with gear box)	Power	250 W
	Voltage	25-28 DC
	Current	9.5 A
	Rated speed(gear box)	340 RPM
Driver sprocket	Number of teeth	36
	Pitch	12.7 mm
Driven sprocket	Number of teeth	13
	Pitch	12.7 mm
Chain	Pitch	12.7 mm

Table 2.3: Drive train summary

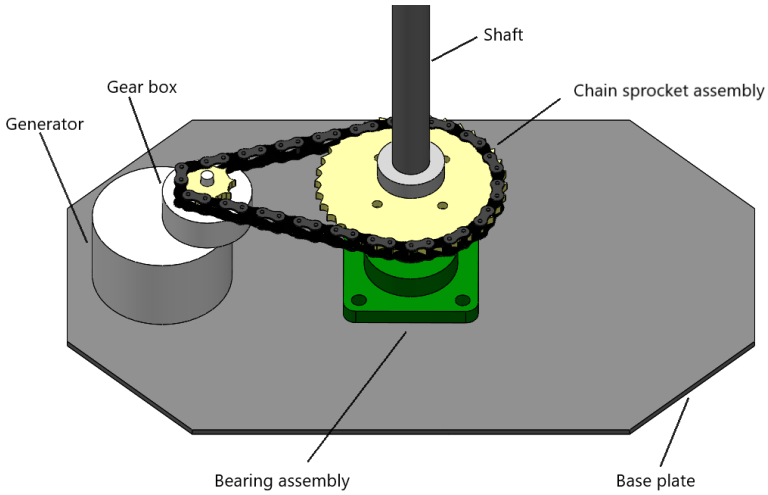

Figure 2.5: Drive train assembly

The generator is an 'off the shelf product' from AEROCATCHER online shop [5]. It is chosen after an extensive market survey performed considering the requirements and objectives of the competition. The chosen generator is a 250 W with 25-28 V DC output with an integrated gear box. The maximum current capacity is 9.5 A. The rated speed of the generator is 2750 RPM, but with the integrated gearbox of ratio 7.2, it reduces to 340 RPM. The rotational speed of our turbine at average wind speeds is calculated from the Weibull parameters provided by the contest organizers is comparatively lower than the generator rated speed. Therefore, a further reduction of 2.7 is achieved through the chain-sprocket assembly. Chain-sprocket is used instead of direct gear drive as the integrated gear box has an output shaft with a sprocket for transferring torque. The chain- sprocket assembly is kept in between two radial load bearings so as to protect it from deflections due to vibrations created by the rotation of turbine. Calculations on structural integrity of the shaft and the drive train is shown in chapter 4.

2.3.3. Safety & Braking

The braking system involves a combination of mechanical braking of the rotor assembly and dynamic braking of the generator. For mechanical braking, the brake disc is mounted on the main shaft, above the base plate as shown in the Figure 2.6. This mechanical brake is the one used in mountain bikes, which have an average braking torque available in a wide range. For instance, the model TRP G-Spec Quadiem has an average torque of 66.2 Nm with the brake disc of 180 mm diameter.

The braking torque and force required to bring the turbine to rest are calculated at the rated angular speed, ω_{rated}, which equals 12.31 rad/s. The torque, Q_{brake} required to bring the turbine to rest is given by Equa-

tion 2.1. The angular deceleration, α, required to bring the rotor to rest from ω_{rated} , within a time interval of 3 s is 4.103 rad/s^2.

$$Q_{brake} = I \cdot \alpha \tag{2.1}$$

The mass moment of inertia,I of the rotor assembly is from the CAD tool is 6.43 $kg{\cdot}\mathrm{m}^2$. Thus, the braking torque required to bring the turbine to rest is 26.382 Nm. The braking force, F_{brake} is found to be 293 N, with Equation 2.2, where r is the radius of the brake disc.

$$F_{brake} = \frac{Q_{brake}}{r} \tag{2.2}$$

The cable for the brake caliper is reeled in (braking) or out (releasing the brake) using a motor. This motor receives the braking command from the Arduino micro-controller.

To assist this mechanical braking and for redundancy in case of failure, dynamic braking of the generator is implemented. Dynamic braking or rheostatic braking of a generator means shorting or connecting a very low resistance across the terminals of a generator whilst the rotor is rotating, thereby increasing the armature current and hence the generator torque T_{gen}. This is executed by connecting the terminals of the generator to a relay controlled by Arduino that gives the circuit open/close command to the relay.

Revolutions per minute, RPM, of the turbine is obtained by attaching a neodymium magnet to the rotating base-end plate of the turbine and positioning a hall effect sensor attached to the stationary frame, such that the magnet passes over it once every rotation. The sensor records these passes as pulses and the time between two subsequent pulses is the time for one rotation. An HC-05 bluetooth module is used for communicating the RPM data to the remote user device and for receiving the emergency brake command from the user. This module has a range of around 10 m.

In case of an emergency braking command from the user or automatic braking over the cut-out winds, the Arduino commands the braking signal, deploying both braking mechanisms.

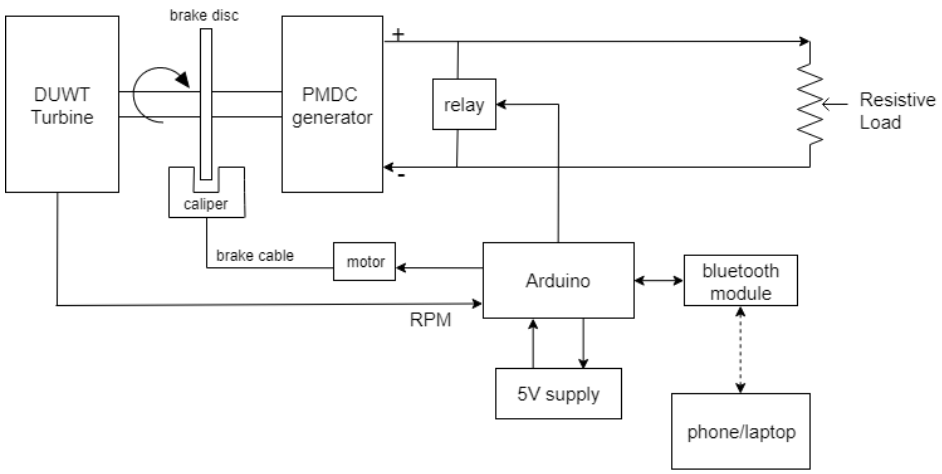

Figure 2.6: Automatic braking schematic

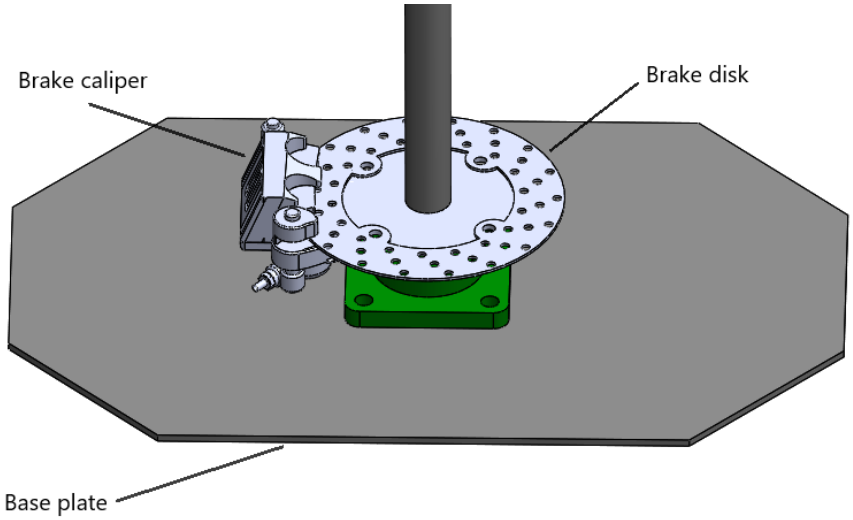

Figure 2.7: Mechanical brake assembly

2.3.4. Control Strategy

The primary aim of the controller is to maintain a constant tip speed ratio in the partial load region, so as to operate at the maximum power point. For the given rotor design, the maximum power coefficient and the corresponding tip speed ratio is obtained. The optimal tip speed ratio determines the operating rotational speed for a particular wind speed value. In the partial load region, the torque at any given rotational speed can be determined using Equation 2.3. It should be noted that the torque and rotational speed values in the equations are at the high speed shaft (HSS) as the torque at the high speed shaft, at the generator end, can be controlled.

$$T_{HSS} = k_{opt} \cdot \omega_{HSS}^2 \tag{2.3}$$

Here, k_{opt} is the optimal mode gain, given by Equation 2.4, in which $\eta_{gearbox}$ is the gearbox efficiency, R is the rotor radius, $r_{gearbox}$ is the gearbox ratio and λ_{design} is the design/optimal tip speed ratio.

$$k_{opt} = \frac{\rho \cdot C_{P,max} \cdot \eta_{gearbox} \cdot H \cdot R^4}{r_{gearbox}^3 \cdot \lambda_{design}^3} \tag{2.4}$$

In Figure 2.8, the red points correspond to the maximum C_P points for different wind speeds (cut in to cut out), while the blue line simply passes through these optimal operating points.

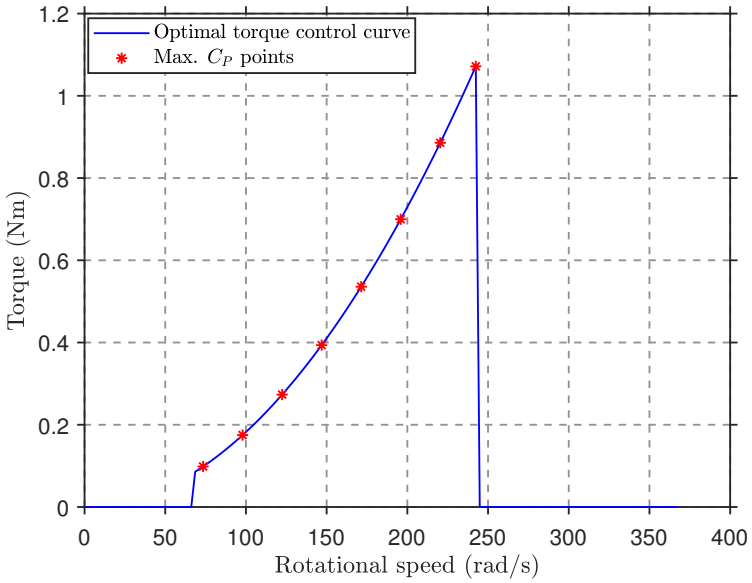

Figure 2.8: Optimal torque control curve

Figure 2.9 shows the schematic of this control strategy. The Arduino receives the rotational speed of the turbine and computes the required generator torque as per Equation (2.3). The relation between generator torque (T_{HSS}) and the armature current I_A is given as

$$T_{HSS} = K_T \cdot I_A \tag{2.5}$$

where K_T is the generator torque constant. Using this equation, the torque requirement is converted to a current requirement. The armature circuit consists of a rheostatic resistive load and an N-channel Power MOSFET. The MOSFET receives a Pulse Width Modulation (PWM) signal from the Arduino. PWM signal is a square wave signal. Duty cycle is the percentage of time in one time period of the wave, for which the signal is in the high state or 5 V. For the remainder of the time period it is in the low state or 0 V. A high state of the signal means the MOSFET shall close the circuit, i.e., current flows in the circuit. While low state means the circuit is open. By changing the duty cycle of the PWM signal, the consequent switching of the MOSFET is used to control the current in the circuit. The resisitve load is used to set the value of max current that can flow in the circuit, i.e., current corresponding to 100% duty cycle.

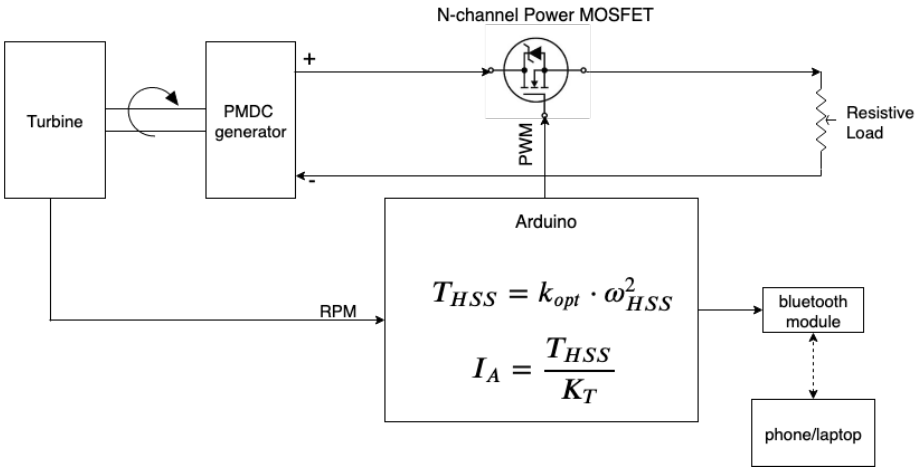

Figure 2.9: Torque Control Schematic

3

Flow Analysis

This chapter is concerned with the utility of two dimensional computational flow analysis as a tool to evaluate the Savonius rotor performance. Viscous unsteady flow simulation over the rotor configurations under varying tip speed ratios is performed. The results indicating the power coefficient and fluid flow visualization are analyzed with emphasis on the highlighting the physical changes in the flowfield due to geometrical modifications.

3.1. Problem set-up

A commercial CFD solver ANSYS Workbench® is used for a complete viscous unsteady solution of incompressible flow around the 2D Savonius rotor configuration. The governing flow equations are the Reynolds-averaged Navier Stokes (RANS) equations. The 2D computational domain is shown in Figure 3.1, where the distance from the rotor origin to the domain inlet and outlet are $12D$ and $24D$, respectively, where D is the diameter of the rotor. The domain is further split into three subdomains with varying refinement of grid elements ensuring numerical accuracy.

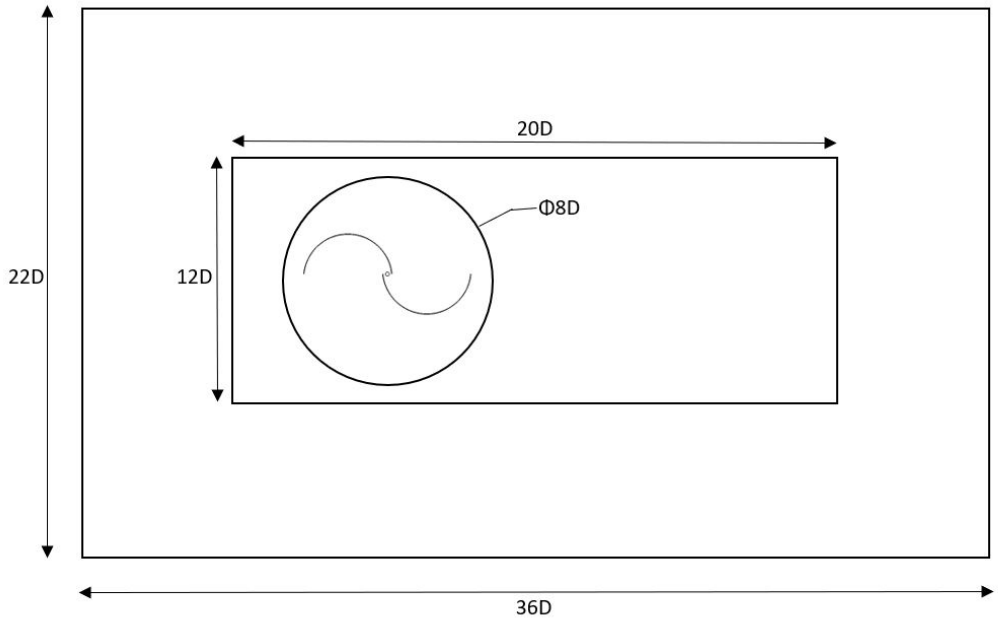

Figure 3.1: A schematic of the computational domain employed for the present numerical simulation

The computational grid consists of quadrilateral cells with minimum y^+ value of 1 on the rotor blade walls. Boundary conditions are: a uniform velocity at the inlet, zero gauge static pressure at the outlet, no-slip walls for rotor blade surfaces, interface between the rotating subdomain around the rotor blades and the fixed region of the domain. A numerical setup similar to [6] is followed. The RANS solution is obtained using the coupled algorithm; it offers robustness and faster convergence for unsteady flows as compared to segregated solution schemes. A least-squares cell based method is used to evaluate the pressure gradient, with pressure and momentum equations solved using a second order upwind differential scheme. The convergence criteria is set to 10^{-6} for all the residuals. A typical converged unsteady RANS solution with approximately 0.2 million mesh elements is obtained in roughly 2.5 hours on a multi-core work-station desktop computer.

The k-ω SST (shear stress transport) model is used as turbulence model for its ability to model separated flows for moving reference frames. The model is well suited for applications wherein vortex shedding due to a rotational domain has an impact on the overall aerodynamic performance. A turbulence intensity of 1% and length scale $0.07L$ are employed for accurate prediction of separation over the surface of the rotor blades. Preliminary investigations showed good agreement with previous numerical investigations [7].

RANS solutions are sensitive to the discretization of the computational domain. For the present computations, an O-grid unstructured zonal approach is chosen (Figure 3.2), which proved to be advantageous in the case of a curved boundary layer, i.e, blade surface. The O-grid loop terminates in the wake region. A sliding mesh approach has been used to simulate the motion of the Savonius rotor blade. The time step for each iteration has been chosen in such a manner so as to rotate the blade by 1° in every iteration. For the validation study, tip speed ratio (TSR) was varied from 0.6 to 1.2 with increments of 0.2. The analytical expression for TSR is given by:

$$\lambda = \frac{D \cdot \omega}{2U} \tag{3.1}$$

where λ is the TSR of the blade, D is the rotor diameter and U is the freestream velocity.

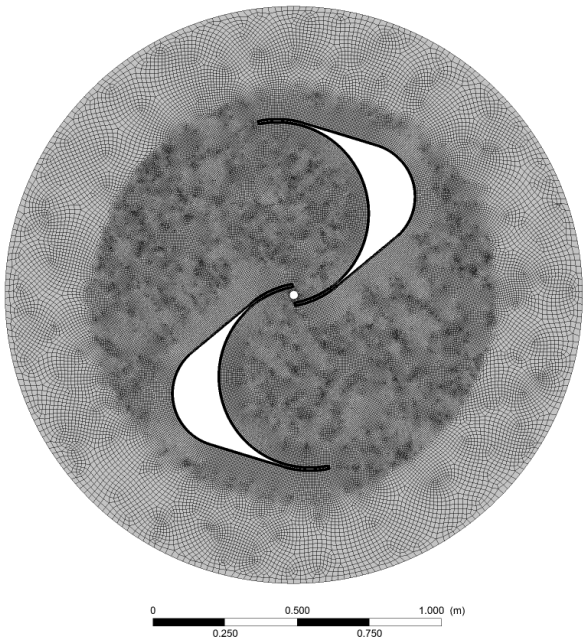

Figure 3.2: Close up view of the grid resolution in the rotating domain

Grid independence is carried out using three grid sizes where the refinement factor in each direction is approximately 1.5. Refinement factor is defined as the rate at which the grid size increases. The resultant moment at the axis of rotation in the positive z direction is taken as reference for the convergence analysis. The

results of the grid independence study are shown in Table 3.1. Convergence is reached for the medium grid, which is then used for the flow analysis of different configurations.

Grid	**Number of cells**	C_m
Coarse	67640	0.3012
Medium	202008	0.3133
Fine	561028	0.3135

Table 3.1: Grid statistics for grid independence study of the reference case.

3.2. Numerical Validation

For validating the numerical approach, the computational model employed by Tian et al [8] is simulated. Tian et al's work involved the computational analysis of a modified Savonius wind turbine using the Myring equation to parametrize the shape of the rotor blades:

$$y = b\left[1 - \left(\frac{x}{a}\right)^2\right]^{\frac{1}{n}} \tag{3.2}$$

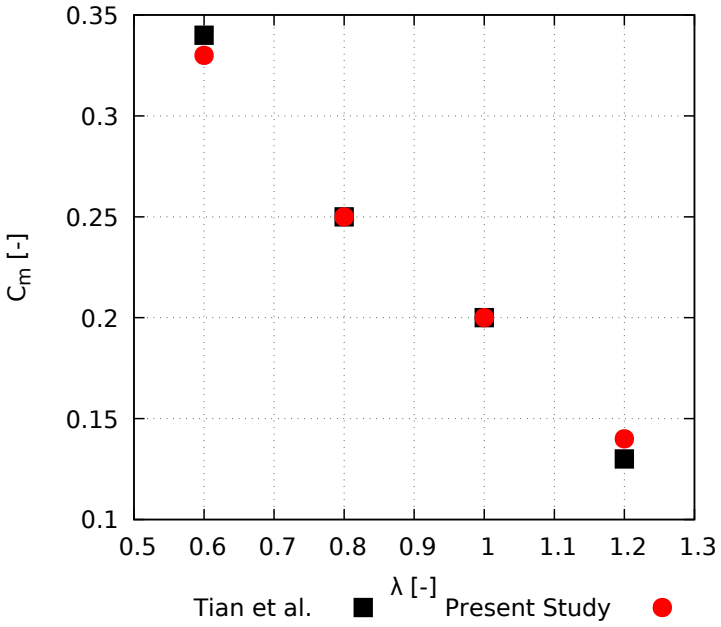

Figure 3.3: Variation in coefficient of torque C_m as a function of TSR λ

The shape of traditional Savonius blades is obtained by substituting $a = b$ and $n = 2$ in the above equation. For the validation study, $a = b = 0.25m$ is used. A TSR ranging from 0.6 to 1.2 is employed for the validation study. The diameter of the Savonius rotor configuration for the validation study is set to $1m$. To match the computational setting used by Tian et al, the grid discretization scheme was changed. However the solver settings were kept the same. The coefficient of torque is used as the reference parameter for comparison.

$$C_m = \frac{M}{0.25 \cdot \rho \cdot S \cdot U^2} \tag{3.3}$$

Here, C_m is the coefficient of torque, M is the instantaneous torque averaged over five revolutions of the rotor system, U is the freestream velocity and S is the cross sectional area swept by the rotor blades, given by $S = D \cdot H$. For the two dimensional simulations, an assumption of $H = 1m$ is made.

The comparison of C_m with λ is shown in Figure 3.3. The deviation from the experiment is 0.8 - 1.1%. The reason is likely due to a difference in the applied turbulence model. Nevertheless, the computed C_m shows a trend in good agreement with previous numerical simulations.

3.3. Results and Discussion

3.3.1. Global Performance Coefficients

To analyze the performance of the two Savonius rotor configurations, global performance coefficients, i.e. moment and power coefficients, are used to quantify the impact of varying the blade profile. Figure 3.4 shows the correlation between C_m and λ for the two blade profiles. The average torque decreases with an increase in λ. The modified Savonius configuration with foam has a higher average torque as compared to the bare rotor configuration due to an additional impedance produced by a thicker blade cross section. Savonius rotor configurations are characterized by a rapidly fluctuating value of instantaneous torque due to the drag based nature of the device. Consequently, fatigue over the span of the rotor blade is relevant to the choice of rotor configuration. The fluctuations in instantaneous torque at $\lambda = 0.8$ are more enhanced for the bare configurations as compared to that of the modified configuration, leading to the latter being preferred from a structural perspective.

Figure 3.4 shows the correlation between the coefficient of power C_P and λ. C_P is defined by the following analytical expression:

$$C_P = \frac{P}{0.5 \cdot \rho \cdot S \cdot U^3} = \lambda C_m \tag{3.4}$$

where P is the total power output by the rotor configuration.

From Figure 3.4, we can ascertain that the modified blade geometry displays greater performance in comparison to the bare rotor configuration for all values of TSR. The peak performance of both rotor configurations is displayed at $\lambda = 0.8$.

3.3.2. Flowfield Analysis

This subsection deals with the analysis of contours of normalized velocity in the vicinity of the rotor blade surfaces. The physical details of the flowfield are discussed from a purely aerodynamic perspective. It is important to note that the definition of bound vorticity is assumed to be constant over both the bare and modified blade geometry.

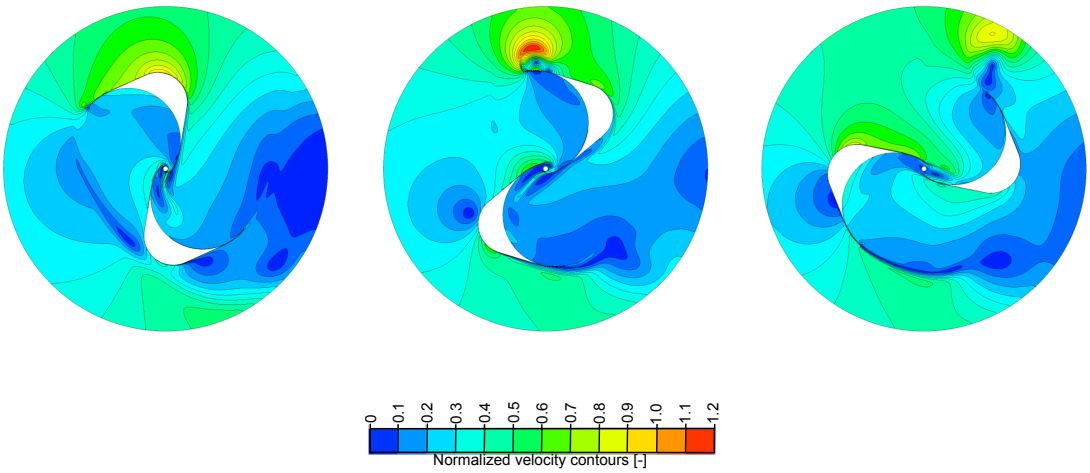

Figure 3.5: Contours of normalized velocity at t = 0.5 s (left) 1.5 s (middle) and 2.5 s (right)

On analyzing the velocity contours for the two rotor configurations (normalized velocity contours for the modified geometry are shown in Figure 3.5), the trend between C_m and λ and between C_P and λ can be explained on the basis of the recirculation zone created on the convex part of the blade surface. The bare rotor geometry experiences a lesser velocity growth in the concave region as compared to that of the modified rotor geometry, thereby leading to a greater resultant torque of the latter. The phenomenon of velocity growth and its impact on resultant torque was also discussed by Kacprzak et al [9]. Moreover, the effect of an 'overlap' jet is significant at those azimuth angles wherein the advancing and retreating blades are perpendicular to the direction of freestream velocity. Another significant aspect of the flowfield observed for both configurations are the vortical structures shed from the blade tips, creating the wake of the Savonius wind turbine. The structure of this vortex shedding is analogous to the Von Karman vortex, and is not observed to be dependent on the rotor blade configuration. The analysis of the flowfield between the bare rotor configuration versus the modified rotor configuration yielded a number of conclusive results: the modified Savonius rotor geometry has a higher efficiency measured in terms of coefficient of power C_P due to a greater recirculation and velocity growth as compared to the bare case; secondly, the added curvature yields to a favorable wake deficit thereby increasing the instantaneous torque. For reducing the computational complexity of the numerical simulations, the geometrical modifications discussed in the subsequent paragraph are carried out for the modified Savonius configuration owing to its greater performance.

Mahmoud et al [7] studied the effect of of blade aspect ratio, overlap and gap between the rotor blades experimentally. It was then found that the rotor configuration without overlap gives a higher mechanical power as compared to the configurations without overlap. To corroborate the findings of Mahmoud et al with the present design configuration, the effect of varying the gap between the blades is numerically investigated. As explained in the preceding paragraph, the effect of the overlap jet was seen to be beneficial for generating a velocity growth in the concave region of the blade surface thereby leading to a greater efficiency of the modified blade geometry. To highlight the beneficial impact of this overlap jet while also considering minimal gap between the two blades, the effect of varying the tip gap on the aerodynamic performance is investigated at $\lambda = 0.8$. The performance of the configurations under varying gap and separation is summarized in Table 3.2.

Configuration	C_P
0 mm Gap and 32 mm Separation	0.265
0 mm Gap and 64 mm Separation	0.269
100 mm Gap and 64 mm Separation	0.254
100 mm Gap and 120 mm Separation	0.242

Table 3.2: Variation of turbine configuration efficiency with tip gap and separation.

On the basis of the present analysis, the modified Savonius configuration with no gap and $64mm$ separation is chosen as the optimum configuration owing to its torque and power characteristics. The additional curvature due to the foam structure yielded a greater efficiency of the 2D rotor in comparison to the bare configuration. Peak power output is witnessed at TSR = 0.8, which is set as the operational TSR for the present design configuration.

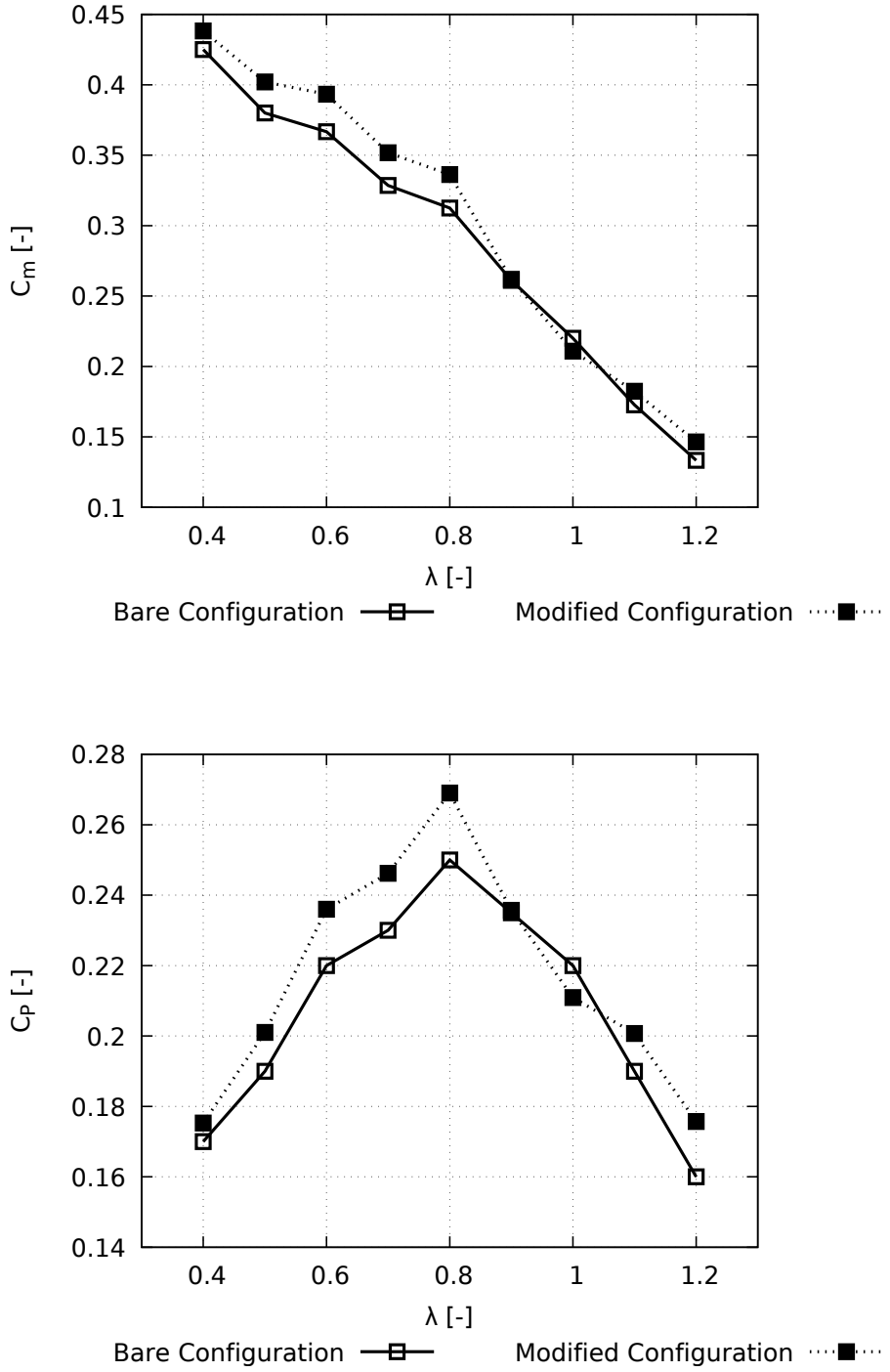

Figure 3.4: Variation in (top) coefficient of torque C_m and (bottom) coefficient of power C_P as a function of TSR λ, respectively

4

Structural Analysis

4.1. Loading Conditions and Analysis

To begin the discussion of the loading cases, the operational envelope of the turbine must be discussed. The turbine must be able to stand up to wind speeds of 15 m/s without sustaining damage or failing. However, our self imposed operational window limits the electrical generation of the turbine to under 10 m/s. Above this speed the turbine will be stopped, and must only stand up to static loading.

With these operational conditions set, the loading conditions can be broken down into several subsystems, each with a set of loading conditions. The subsystems are:

- Turbine Blade
- Turbine End Plates
- Main Shaft
- Drive train

4.1.1. Turbine Blades

The turbine blades are exposed to two loading conditions - Bending due to a pressure differential, and inertial loading.

Bending The turbine blades for a Savonius can be considered a simply supported beam subjected to a uniform load. As such, simple beam bending calculations apply to this scenario. The deflection of the center of the blade is given by the equation:

$$\delta_c = \frac{5}{384} \cdot \frac{wL^3}{E \cdot I_{Area}} \tag{4.1}$$

where w is the load, L is the beam length, E is the material stiffness, and I, the Area Moment of Inertia, is given by:

$$I_{Area} = 0.1098 \cdot (R_{outer}^4 - R_{inner}^4) \tag{4.2}$$

Here R refers to radius.

The distributed loading of the blade is equivalent to a centrally located point load of 319 N. As failure of this component would be catastrophic to the integrity of the turbine and potentially damaging to nearby people or objects, a safety factor of 2 is applied to the load, giving a load of 638 N. The morphology of this turbine gives a R_{outer} value of $0.342m$, and a thickness of $0.002m$ gives an R_{inner} value of $0.340m$. When substituting into Equation 4.2, this gives an area moment of inertia of:

$$I_{Area} = 0.1098 \cdot (0.342^4 - 0.340^4) = 0.0001497672m^4 \tag{4.3}$$

This gives a center point deflection of:

$$\delta_c = \frac{5}{384} \cdot \frac{638N \cdot 1.3m^3}{68.9GPa \cdot 0.0001497672m^4} = 1.768e^{-6}m \tag{4.4}$$

The stress, σ, due to this loading condition is calculated via:

$$\sigma = \frac{M \cdot y}{I_{Area}} \tag{4.5}$$

Where M is the applied Bending Moment and y is the distance from the neutral axis. However, the neutral axis of this beam is not located halfway through it's thickness due to its unbalanced construction. The height of the neutral axis is calculated with the equation:

$$y = \frac{4 \cdot (R_{outer}^3 - R_{inner}^3)}{3\pi \cdot (R_{outer}^2 - R_{inner}^2)} \tag{4.6}$$

Substituting into this equation gives us a neutral axis height of **y = 0.217088** m.
Utilizing this height, our max stress is calculated as:

$$\sigma = \frac{199.375Nm \cdot 0.217088m}{0.0001497672m^4} = \textbf{0.288 MPa} \tag{4.7}$$

Inertial The inertial loads present themselves as a lateral bending load from the centrifugal forces. The bending moment is calculated via:

$$M = \frac{1}{2} \frac{m_{blade} \cdot v_{wind}^2}{R} \cdot \frac{L_{blade}}{2} \tag{4.8}$$

Where m_{blade} is the mass of the blades, v_{wind} is speed of wind and L_{blade} is length of blade and R is the radius of the center of the blade. Plugging this into Equation 4.7, we get a stress of:

$$\sigma = \textbf{0.375 MPa} \tag{4.9}$$

4.1.2. Turbine End Plates

The major loading condition of the end plates are derived from the carry of the torque, and the transfer to the main shaft through the flange bolts. These bolt holes need to be able to transfer this torque without experiencing a bearing failure of the bolt hole.

The primary failure methods to be concerned with would be a shear-out type failure or a net section failure. Both of these will be calculated against with a 4 bolt pattern, located on a 100 mm diameter circle utilizing M5 bolts. The operation torque of the turbine is 21.75 Nm of torque.

Shear-out The shear- out failure is calculated as the force applied over the bearing area, in this case the lateral area of the hole.

$$\sigma_b = \frac{F}{A_b} \tag{4.10}$$

For the end plates, the Force, F and Area, A_b are calculated as:

$$F = \frac{\tau}{radius} = \frac{5.4375Nm}{0.05m} = 108.75N \tag{4.11}$$

Here, τ is the applied torque.

$$A_b = \pi \cdot \frac{d}{2} \cdot h = \pi \cdot 0.0025m \cdot 0.002m = 1.57 \cdot 10^{-5}m^2 \tag{4.12}$$

Here, d is the diameter of the bolt hole and h is the thickness of the plate. This gives a Bearing Stress of:

$$\sigma_b = \frac{F}{A_b} = \frac{108.75N}{1.57 \cdot 10^{-5}m^2} = \textbf{6.21 MPa} \tag{4.13}$$

Net Section Failure The Net Section Failure is calculated with:

$$\tau = \frac{F}{A_{shear}} \tag{4.14}$$

Where τ is the shear stress and F is the applied load. In this instance, however, the shear area is the circle area that the bolts are all placed on. This gives a net section stress of:

$$\tau = \frac{\frac{21.75Nm}{0.05m}}{\pi \cdot 0.1m \cdot 0.002m} = \mathbf{0.621\ MPa} \tag{4.15}$$

4.1.3. Main Shaft

The main shaft is responsible for transmitting the torque from the rotor to the generator and sustaining the bending moment associated with exposing the turbine to the wind. As stated above, the turbine generates 21.75 Nm of torque at its max operating condition. This torque is transmitted to the main shaft via two flanges, one at the top of the rotor and one at the bottom. The bending moment that the shaft is subjected to waivers between a maximum when the plane generated by the leading edges of the two blades is perpendicular to the wind speed, and a minimum when is it parallel to it. This bending moment can be calculated based on the drag generated by the turbine and its distance from the support of the shaft. The force is calculated via the standard drag equation:

$$F = \frac{1}{2} \cdot C_d \cdot \rho \cdot V^2 \cdot A \tag{4.16}$$

Where C_d is the drag coefficient, ρ is the air density, V is the Air Velocity and A is the projected area.

The Drag Coefficient for our turbine is

- 1.2 for Perpendicular to the flow
- 0.6 for Parallel to flow

This leads to Applied forces of:

$$F_{perpendicular} = \frac{1}{2} \cdot 1.2 \cdot 1.225kg/m^3 \cdot (15m/s)^2 \cdot (1.25m \cdot 1.3m) = 268.73N \tag{4.17}$$

$$F_{parallel} = \frac{1}{2} \cdot 0.6 \cdot 1.225kg/m^3 \cdot (15m/s)^2 \cdot (1.3m \cdot .625m) = 67.18N \tag{4.18}$$

When coupled with our shaft dimensions, we have a maximum bending moment of

$$M_{perpendicular} = F \cdot d = 268.73N \cdot .645m = \mathbf{173.33\ Nm} \tag{4.19}$$

$$M_{parallel} = F \cdot d = 67.18N \cdot .645m = \mathbf{43.33\ Nm} \tag{4.20}$$

Now that the loads have been determined, the stresses on the shaft can be analyzed. At the top of the turbine, there will be no bending moment, only an applied torque. This torque is transferred to the main shaft via a 5 mm dowel pin driven through an according hole. The Stress Concentration Factor, K_t ,associated with this hole can be calculated by

$$K_t = C_1 + C_2 \cdot \frac{2r}{D_{outer}} + C_3 \cdot \left(\frac{2r}{D_{outer}}\right)^2 + C_4 \cdot \left(\frac{2r}{D_{outer}}\right)^3 \tag{4.21}$$

where

$$C_1 = 4.0 \tag{4.22}$$

$$C_2 = -6.055 + 3.184 \cdot \frac{D_{inner}}{D_{outer}} - 3.461 \cdot \left(\frac{D_{inner}}{D_{outer}}\right)^2 \tag{4.23}$$

$$C_3 = 32.764 - 30.121 \cdot \frac{D_{inner}}{D_{outer}} + 39.887 \cdot \left(\frac{D_{inner}}{D_{outer}}\right)^2 \tag{4.24}$$

$$C_4 = -38.330 + 51.542 \cdot \sqrt{\frac{D_{inner}}{D_{outer}}} - 27.483 \frac{D_{inner}}{D_{outer}} \tag{4.25}$$

Giving a value of

$$K_t, top = 5.37 \tag{4.26}$$

and a maximum stress of

$$\sigma_{max} = K_t \cdot \tau_{nom} = K_t \cdot \frac{16 \cdot T \cdot D_{outer} \cdot S.F}{\pi (D_{outer}^4 - D_{inner}^4)} = \mathbf{50.54\ MPa} \tag{4.27}$$

If we were to place this same dowel pin on the lower connection, the shaft would fail due to the bending moment, as the stress, accounting for the stress concentrator, would be **512.82 MPa**. As such, this joint will be welded. However, to allow for larger safety margins, the shaft will only be welded on the sides that correspond to the parallel bending condition calculated in Equation 4.20, as that is much lower.

To start, the length of weld must be determined. The specified welds are 5 mm fillet welds. This corresponds to a throat thickness of **3.53 mm**. To calculate the weld length needed, we need an approximation of the strength of the weld. For this, as weld efficiency factor of 0.50 was used, as the shaft is a work-hardenable alloy of steel, and this is in line with aerospace recommendations. The length of the weld bead can then be solved for using the following equation

$$\tau = \frac{\frac{2 \cdot T}{D_{outer}}}{h \cdot L} \tag{4.28}$$

Where T is the applied torque, h is the weld throat thickness and L is the weld length. If we rearrange to solve for L

$$L = \frac{\frac{T \cdot S.F}{D_{outer} \cdot 0.5}}{h \cdot \tau} = \frac{\frac{10.875 Nm \cdot 2}{0.015 m}}{0.00353 m \cdot 220 MPa \cdot 0.50} = \mathbf{3.73\ mm} \tag{4.29}$$

As it is obvious, this is a very small weld length, and the weld in practice will be near 5 mm per side. However it is promising, as the heat affected zone will not influence the tube in the highest stress region due to the bending moment in the perpendicular condition.

For this loading condition, we apply the aforementioned moment of 173.33 Nm. This bending moment can be used in the equation below

$$\sigma_{bending} = \frac{M \cdot y \cdot S.F.}{I_{Area}} \tag{4.30}$$

Where M is the bending moment, y is the distance from the central axis, and $S.F.$ is the safety factor. Substituting in the geometrical properties of our shaft, we can solve for stress due to this.

$$\sigma_{bending} = \frac{173.33 Nm \cdot 0.015 m \cdot 1.25}{1.73 e^{-8} m^4} = \mathbf{187.85\ MPa} \tag{4.31}$$

4.1.4. Drive Train

The drive train main sprocket is coupled to the main shaft via a **5 mm** dowel pin. The stress concentration factor is calculated above for the main shaft. Taking that same factor, 5.37, we can now verify the safety of the main shaft at this point. Because this part of the shaft is simply supported by the support structure, the bending moment will be minimal in this zone. As such, only the torsion applies. Two things need to be checked:

- The ability of the dowel pin to carry this load
- The safety of the shaft from this load and concentrator

The dowel pin will carry this load in shear. The formula for this shear stress is:

$$\tau_{pin} = \frac{F}{A} = \frac{F}{\pi \cdot r_{pin}^2} \tag{4.32}$$

where

$$F = \frac{T \cdot S.F.}{r_{shaft}} \tag{4.33}$$

This gives us a stress of

$$\tau_{pin} = \frac{T \cdot S.F.}{\pi \cdot r_{pin}^2 \cdot r_{shaft}} = \mathbf{148.54\ MPa} \tag{4.34}$$

Now, we calculate the stress in the shaft due to this load. This is done with the torsional stress equation,

$$\tau_{shaft} = \frac{Tr \cdot S.F.}{J} \cdot K_t = \frac{21.75Nm \cdot 0.015m \cdot 2}{3.47e-8m^4} \cdot 5.37 = \mathbf{100.97\ MPa} \tag{4.35}$$

4.1.5. Margins of Safety

Here, all the calculated stresses are tabulated and safety margins are calculated. The two materials used for the construction of the turbine are Aluminum 1050A H14 and EN220 grade steel. The yield strengths of the two materials are

- Aluminum 1050A H14 - Yield Strength: 105 MPa
- EN220 Steel - Yield Strength: 220 MPa

Margin of Safety is calculated using the equation

$$M.S. = \frac{\sigma_{allowable}}{\sigma_{Applied}} - 1 \tag{4.36}$$

Components	Load State	Material	Applied Stress	Margin of Safety
Turbine Blades	Flap-wise Bending	Aluminum	0.228 MPa	465.6
	Edge-wise Bending	Aluminum	0.375 MPa	279
End Plates	Shear Out	Aluminum	6.21 MPa	15.91
	Net Section Failure	Aluminum	0.621 MPa	159.08
Main Shaft	Upper Dowel Pin	Steel	50.54 MPa	3.35
	Bending Stress	Steel	187.85 MPa	.17
Drivetrain	Dowel Pin Stress	Steel	148.54 MPa	.48
	Torsional Stress	Steel	100.97	1.17

Table 4.1: Table of Loads and Margins of Safety

4.2. Campbell Diagram

The Campbell diagram serves as a tool to assess possible resonance frequencies in the turbine structure. Based on the rotational speed range and the natural frequencies of the blades, a MATLAB code is generated to built the diagram shown in Figure 4.1. The natural frequencies are obtained using the Computer Aided Design (CAD) model of the blades and performing a Modal Analysis in ANSYS Structural. Only the first lead-lag and flap modes are considered in our analysis. On the other hand, the fore-aft mode of the supporting structure is introduced. Table 4.2 provides the natural frequencies from these simulations, which are based on the geometry of the blades and the constraints (supports). These natural frequencies correspond to non-rotating elements. Therefore, centrifugal stiffening is considered to account for the additional stiffening produced from the rotation of the blades. This correction is obtained by using Table 4.2.

Mode	Value (rad/s)
Flap	136.3
Lead-lag	241.9
Fore-aft	377.0

Table 4.2: Different Mode Shapes of the Savonius Wind Turbine

$$\omega_{n,Rot}{}^2 = \omega_{n,Non-Rot}{}^2 + K \cdot \omega^2 \tag{4.37}$$

The Equation 4.37 above translates the non-rotating natural frequency to a rotating natural frequency, accounting for centrifugal effects that stiffen the structure. The relationship depicted above introduces a relevant term, K, which is called the Southwell coefficient. In this analysis, a value of 1.8 is established, based on empirical data [10]. No specific information upon Savonius wind turbines centrifugal stiffening could be obtained. However it is considered a conservative estimation, since all the modes are higher than the 1P, 2P, 3P range. Figure 4.1 shows the resulting Campbell diagram for the Savonius wind turbine.

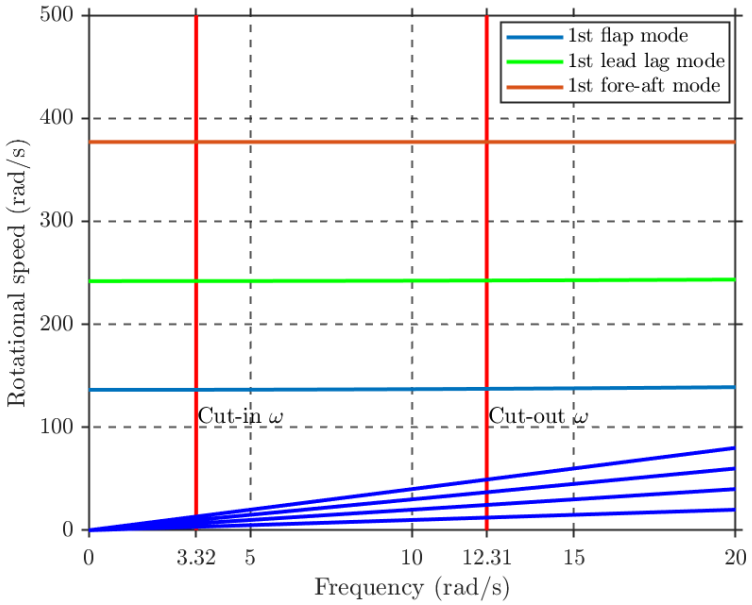

Figure 4.1: Campbell Diagram of the Savonius Wind Turbine

In this diagram, only the 1P, 2P, 3P and 4P excitation frequencies are considered, as it is a 2-bladed turbine. Furthermore, 5P and above are neglected in this study, as they represent a low energetic content for possible resonance based on the wind speed range that it is operating. On the other hand, the rotational speed range is 3.32 rad/s to 12.31 rad/s, based on the cut-in speed and the maximum speed (as there is no control strategy). The figure shows that the mode shapes considered are far above the 1P, 2P, 3P, 4P lines, for the region considered. This implies that no risks upon structure resonance should be encountered under this design.

5

Turbine Specifications

This chapter summarizes the turbine design based on the methodology presented in the preceding chapters. Table 5.1 provides the reader with all the major turbine specifications.

Parameter	**Specification**	**Units**
P_{rated}	268	W
No. of blades	2	-
D_{rotor}	1.3	m
H_{rotor}	1.25	m
A_{rotor}	1.63	m^2
V_{cut-in}	2.7	m/s
V_{rated}	10	m/s
$V_{cut-out}$	10	m/s
Max C_P	0.269	-
λ	0.8	-
T_{rated}	21.75	Nm
ω_{rated}	12.31	rad/s
Drive type	Chain drive	-
Overall gear ratio	26	-
Generator Type	PMDC	-
Generator P_{max}	250	W
Generator η_{max}	84	%
V_{max}	24-28	V
I_{max}	9.5	A

Table 5.1: Turbine specifications

Based on the maximum power-coefficient value and the corresponding tip speed ratio, the power values for the entire wind speed range are determined. The rotational speed values for each of the wind speeds are derived based on the optimal tip speed ratio. Subsequently, the torque values are calculated based on the power and rotational speed values. The torque curve obtained is shown in Figure 5.1a.

The cut-in wind speed, represented by the black line is the speed at which the rotor torque overcomes the resistance torque offered by the generator, which is calculated to be 2.7 m/s. The turbine then traces the optimum power curve where the power at any wind speed is given by Equation 5.1, where a rated wind speed of 10 m/s is chosen, after which, the turbine automatically shuts down. This is done in order to prevent the generator from overheating and keeping the power below the rated limit.

$$P = \frac{1}{2} \cdot C_P \cdot \rho \cdot A \cdot v^3 \tag{5.1}$$

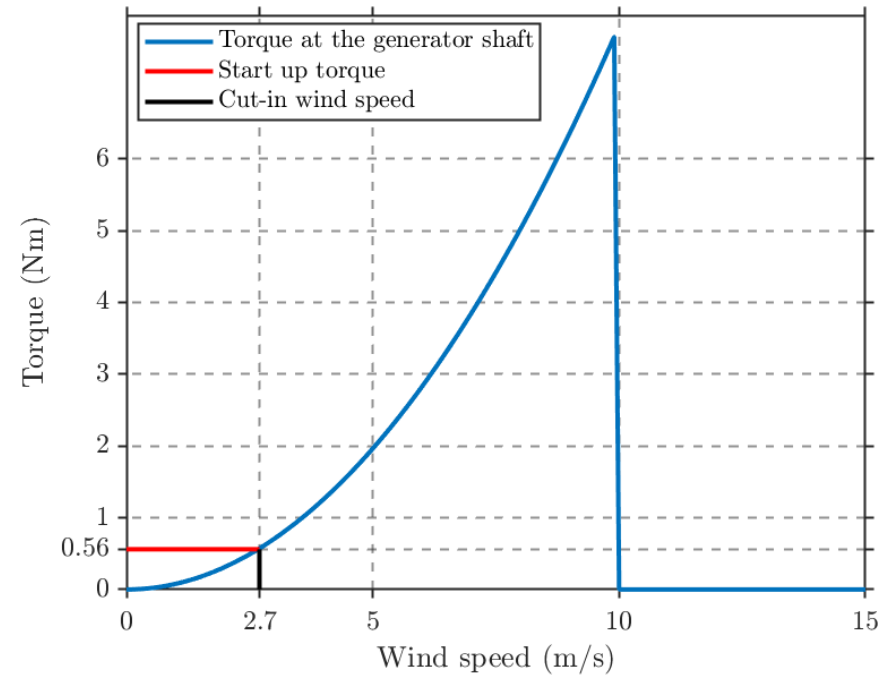

(a) Torque curve of the designed turbine

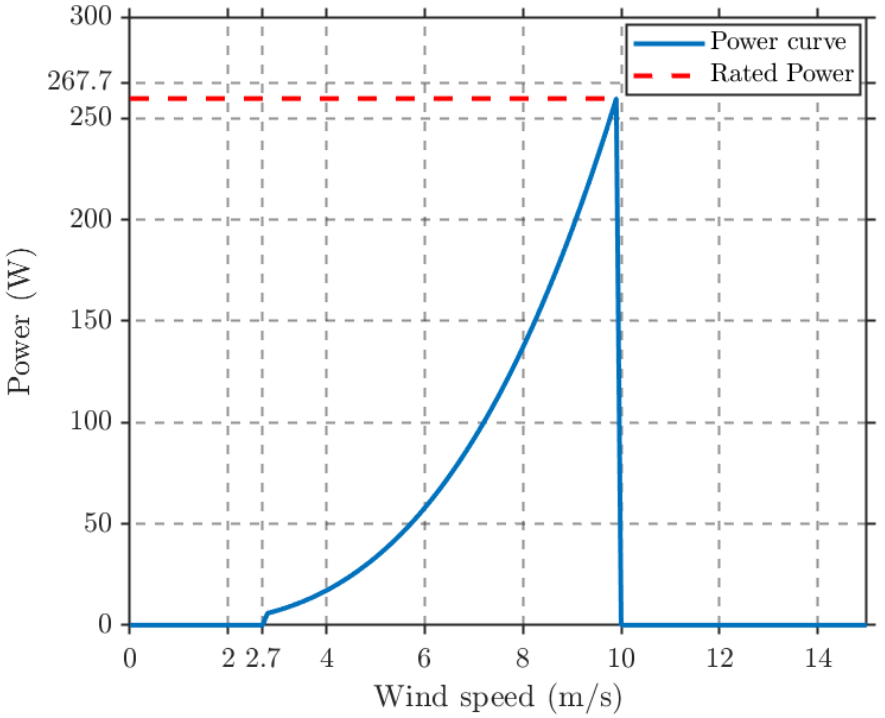

(b) Power curve of the designed turbine

Figure 5.1: Torque curve and Power Curve of the turbine

6

Energy payback period

In this chapter, the energy payback period for the Savonius wind turbine is estimated. The chapter starts off with the basic definition of the energy payback period followed by the estimated energy use for manufacturing the wind turbine. The chapter concludes with the calculation of the annual energy production and the estimated energy payback period. The energy payback period of the wind turbine refers to the time taken for the wind turbine to generate the same amount of energy that is used to manufacture the wind turbine and balance of systems [11].

6.1. Estimated energy use

For estimating the energy used to manufacture the wind turbine, the first step is to list out the system components of the wind turbine. Table 6.1 shows the components of the wind turbine, material used to manufacture the components followed by the estimated weight.

Component	**Material**	**Estimated weight (kg)**
Blades	Aluminium	13.5
End plates	Aluminium	13.1
Driveshaft	Steel	2.3
Drivetrain (sprockets + chain+ flanges + bearings)	Cast iron and steel	17
Generator	Cast iron, steel and copper	11.5

Table 6.1: Wind turbine components

After identifying the material and weights of the components of the wind turbine, the energy used to manufacture each component is calculated. The US Department of Energy has made estimates for the energy used to produce various materials. Table 6.2 shows the energy used to produce the materials pertaining to the wind turbine [12].

Material	**Steel**	**Cast iron**	**Aluminium**
Energy usage (10^6 BTU/ ton)	1.225	1.2	0.986
Energy usage (kWh/kg)	0.359	0.352	0.289

Table 6.2: Material energy [12]

Therefore the energy used to manufacture the components of the wind turbine can be calculated, which is listed in Table 6.3. The total energy used to manufacture the wind turbine is 13.5 kWh.

Component	Estimated energy usage (kWh)
Blades	3.90
Endplates	3.79
Driveshaft	0.83
Drivetrain (sprockets + chain+ flanges + bearings)	6.10
Generator	4.13

Table 6.3: Energy used to manufacture the Wind turbine components

6.2. Annual energy production

The Annual Energy Production (AEP) reflects the amount of energy that is harnessed from the wind turbine based on the site conditions and the power curve, which illustrates the power production under a range of wind speeds. The site conditions are defined in the guidelines of the competition. It corresponds to a Weibull distribution with a scale parameter of $a = 4.5$ and a shape parameter of $k = 2$, the latter being a typical value for Northern Europe [10]. The annual energy production of the turbine can be obtained by multiplying the electrical power of the turbine with the probability density function of the given wind climate. The resultant probability density function obtained using Equation 6.1, is shown in Figure 6.1b.

$$f(U) = \frac{k}{a} \cdot \left(\frac{U}{a}\right)^{k-1} \cdot e^{-\left(\frac{U}{a}\right)^k} \tag{6.1}$$

The generator used has a rated power of 250 W and a maximum efficiency of around 84%, at 2992 RPM. Also, the efficiency drops to 20% for low load conditions. As the exact values of the generator efficiency, as a function of RPM and load, are not known, it is assumed to be operating at around 50% efficiency in the range of 3-7 m/s and around 75% efficiency in the range of 7-10 m/s, based on the operating load in the respective particular wind speed range. This electrical power is then used for energy production calculations.

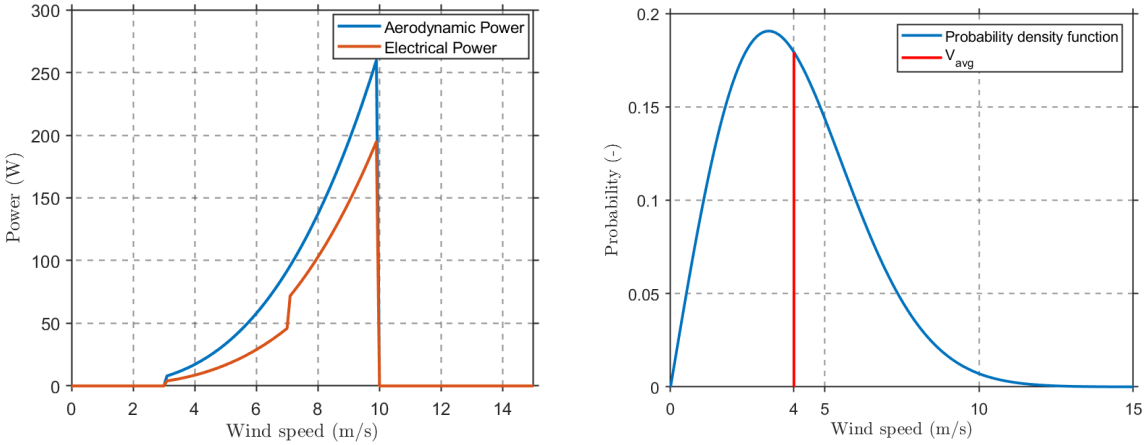

(a) Electrical Power curve of the designed turbine

(b) Given Weibull distribution

Figure 6.1: Electrical Power curve and Weibull distribution

Finally, the annual energy produced by the turbine can be easily obtained using Equation 6.2, where P_{elec} is the electrical power, f is the probability density function, T is the number of hours in a year and dU is the wind speed bin size.

$$E = T \cdot \int_{cut-in}^{cut-out} P_{elec}(U) \cdot f(U) dU \tag{6.2}$$

The energy obtained using Equation 6.2, multiplied with an assumed availability of 90%, gives an annual energy production of 137 kWh, leading to a capacity factor of 0.06. A low capacity factor can be attributed to

the fact that the turbine operates in the range of 10-35 % of the rated load of the generator for wind speeds 4-7 m/s, which have a maximum probability of occurrence. However, as the goal of the competition is to maximize the annual energy production and not minimize turbine the Levelized Cost of Energy, LCOE, the generator is sized based on the power produced at the rated wind speed of 10 m/s.

6.3. Energy payback period

With the estimated energy used to manufacture the wind turbine components and the annual energy production calculated, the energy payback period can then be estimated. The formula used for calculating the energy payback period is shown below.

$$EPP = \frac{E_b + E_e + E_{ds} + E_{dt} + E_g}{AEP} \tag{6.3}$$

where, EPP is the energy payback period in years, E_b is the energy input to make the blades, E_e is the energy input to make the end plates, E_{ds} is the energy input to make the driveshaft, E_{dt} is the energy input to make the drivetrain, E_g is the energy input to make the generator and AEP is the annual energy production. (All units are in kWh)

Using the formula above, an energy payback period of 0.14 years is calculated. This translates to 1.6 months which is equivalent to 49 days. Therefore, in 49 days, the Savonius wind turbine is expected to generate enough energy to break-even with the energy used to manufacture the turbine. Haapala et al, suggests that, for a 2 MW wind turbine, an energy payback period of five to eight months is expected [13]. As the Savonius wind turbine designed for the competition, is at a much smaller scale compared to a 2 MW wind turbine, an energy payback period of 49 days appears reasonable in this context.

7

Conclusion

The main goal of the challenge was to design a fully functional, robust and safe small wind turbine that complies with all the competition requirements. Driven by the values of uniqueness, low cost and functionality as well as the desire to innovate and contribute towards future development and applications of the small wind turbine, DUWT has reached the goal by designing a low cost efficient and safe Savonius wind turbine for this competition.

The focus of the design process resulted in taking optimal choices for the turbine components and subsystems. The interface between different subsystems is thoroughly evaluated to ensure structural integrity and safety, both being the top priorities.

The rotor for the Savonius turbine is simulated for different configurations with respect to the gap and separation, which corroborate the already existing literature on the same. Also, few studies have explored the shape of the blade arc and optimized the same. However, the possibilities of having an additional modified attachment while preserving the conventional optimized shape of the blade arc, which is something that had not been tried out previously is explored in this research.

References

[1] Suri, Dhruv. "Design of an Optimized Inlet Shroud for a Flanged Diffuser." (2019).

[2] Radhakrishnan, Jayakrishnan, and Dhruv Suri. "Design and Optimisation of a Low Reynolds Number Airfoil for Small Horizontal Axis Wind Turbines." *IOP Conference Series: Materials Science and Engineering*. Vol. 377. No. 1. IOP Publishing, 2018.

[3] Suri, Dhruv, Jayakrishnan Radhakrishnan, and Raahil Nayak. "Lattice Boltzmann Method to Analyse Fluid Flow Around a Circular Cylinder." (2019).

[4] Suri, Dhruv. "The Potential for Ducted Wind Turbines in an Urban Environment." (2019).

[5] Dighe, Vinit, et al. "Ducted wind turbines in yawed flow: A numerical study."